Electronic structure of BiMO_3 multiferroics and related oxides

J. A. McLeod,[1,*] Z. V. Pchelkina,[2,†] L. D. Finkelstein,[2] E. Z. Kurmaev,[2] R. G. Wilks,[1] A. Moewes,[1] I. V. Solovyev,[2,3] A. A. Belik,[4] and E. Takayama-Muromachi[4]

[1]*Department of Physics and Engineering Physics, University of Saskatchewan, 116 Science Place, Saskatoon, Saskatchewan, Canada S7N 5E2*

[2]*Institute of Metal Physics, Ural Division, Russian Academy of Sciences, 620990 Yekaterinburg, Russia*

[3]*Computational Materials Science Center, National Institute for Materials Science, 1-2-1 Sengen, Tsukuba, Ibaraki 305-0047, Japan*

[4]*International Center for Materials Nanoarchitectonics (MANA), National Institute for Materials Science (NIMS), 1-1 Namiki, Tsukuba, Ibaraki 305-0044, Japan*

(Received 9 October 2009; revised manuscript received 3 February 2010; published 9 April 2010)

We have performed a systematic study of the electronic structures of the BiMO_3 (M=Sc,Cr,Mn,Fe,Co,Ni) series by soft x-ray emission (XES) and x-ray absorption (XAS) spectroscopy. The band gaps were estimated for all compounds in the series. For $BiFeO_3$, a band gap of ~0.9 eV was obtained from the alignment of the O $K\alpha$ XES and O 1s XAS. The O 1s XAS spectrum of $BiNiO_3$ indicates that the formation of holes was due to a Ni^{2+} valency rather than a Ni^{3+} valency. We have found that the O $K\alpha$ XES and O 1s XAS, probing partially occupied and vacant O 2p states, respectively, are in agreement with the O 2p densities of states obtained from spin-polarized band-structure calculations for all BiMO_3 compounds addressed herein. The O $K\alpha$ XES spectra show the same degree of Bi 6s-O 2p hybridization for all compounds in the series. We speculate herein that the stereochemical activity of the Bi 6s lone pairs must be supplemented with inversion symmetry breaking to allow electric polarization. For $BiMnO_3$ and $BiFeO_3$, two cases of multiferroic materials in this series, the former breaks the inversion symmetry due to the antiferromagnetic order induced by particular orbital ordering in the highly distorted perovskite structure and the latter has rhombohedral crystal structure without inversion symmetry.

DOI: 10.1103/PhysRevB.81.144103 PACS number(s): 71.20.Gj

I. INTRODUCTION

Multiferroics, materials which were discovered almost 50 years ago,[1,2] simultaneously possess two or three degrees of freedom: (anti)ferromagnetism, (anti)ferroelectricity, and/or ferroelasticity. This combination allows both charges and spins to be manipulated by applied electric and magnetic fields.[3,4] These materials are promising for various technological applications such as information storage, spintronics, and sensors. There are many different classes of multiferroic systems known today, for instance, the RMnO_3 family (R=Dy,Tb,Ho,Y,Lu, etc.), the RMn$_2O_5$ family (R=Nd,Sm,Dy,Tb), and the BiMO_3 family (M=Mn,Fe). These materials have complex structures with many atoms per formula unit, and more than one formula unit per unit cell. The large number of interatomic interactions makes distinguishing the mechanisms responsible for multiferroicity a challenging task. The origin of these phenomena and the nature of the coupling between the magnetic, electric, and structural order parameters are not well understood.

For the wide class of transition-metal perovskites, it was determined that magnetism and ferroelectricity seem to exclude one another (for review, see Refs. 5 and 6). In conventional ferroelectric perovskites, the transition-metal ion has d^0 electron configuration and such systems are nonmagnetic. The compounds having electrons in a d-shell may be magnetic but they are not ferroelectric. $BiFeO_3$ and $BiMnO_3$ are multiferroics and are exceptions to this rule. Multiferroicity in these two materials does not break the general "exclusion" rule for perovskites, however. The ferroelectricity in these systems has different source than that in most perovskite ferroelectrics, such as $BaTiO_3$. The driving force for the instability leading to the ferroelectricity in these two cases is the so-called lone pairs of Bi^{3+} ion. The role of lone pairs, ns^2np^0 electron configuration, in such system as $SnWO_4$, $PbWO_4$, $BiVO_4$, and $BiMnO_3$ were addressed in detail in Refs. 7 and 8. The presence of lone pairs leads to an off-centric displacement of the cation from the centroid of it coordination polyhedron. Such asymmetric local environment induces dipoles and give rise to ferroelectricity. For $SnWO_4$, it was shown that the lone-pair distortion leads to a significant increase in the Sn 5s-O 2p bonding interaction. The same tendency was found for $BiVO_4$.[7] This investigation revealed that the stereochemical activity of the lone pairs is exhibited by raising of a cation ns-O 2p bonding interaction. This evidence could be useful for experimental and theoretical analysis of multiferroics and related compounds.

In the present paper, we have performed a systematic study of the electronic structure of the perovskitelike multiferroics ($BiFeO_3$ and $BiMnO_3$) and the BiMO_3 (M=Sc,Cr,Co,Ni) related compounds using synchrotron excited soft x-ray emission and absorption spectroscopy. Despite many electronic-structure calculations (see review article Ref. 9, and references therein), only a few experimental spectra for selected compounds ($YMnO_3$ and $BiFeO_3$) have been obtained so far.[10,11] This could be partially connected with the difficulties in preparing the high-quality samples of these materials which require the high-pressure synthesis. The experimental spectra are compared with specially presented electronic-structure calculations. We also analyze the Bi 6s-O 2p hybridization for the compounds in the series as the possible manifestation of the stereochemical activity of the lone pairs.

TABLE I. Crystal structure and lattice parameters for BiMO_3 compounds.

	$BiScO_3$	$BiCrO_3$	$BiMnO_3$	$BiFeO_3$	$BiCoO_3$	$BiNiO_3$
Space group	$C2/c$	$C2/c$	$C2/c$	$R3c$	$P4mm$	$P\bar{1}$
a, (Å)	9.8899(5)	9.4641(4)	9.5415(2)	5.58102(4)	3.71990(7)	5.3852(2)
b, (Å)	5.8221(3)	5.4790(2)	5.61263(8)	5.58102(4)	3.71990(7)	5.6498(2)
c, (Å)	10.0462(5)	9.5850(4)	9.8632(2)	13.8757(2)	4.71965(15)	7.7078(3)
α, (deg)	90	90	90	90	90	91.9529(10)
β, (deg)	108.300(3)	108.568(3)	110.6584(12)	90	90	89.8097(9)
γ, (deg)	90	90	90	120	90	91.5411(9)

The paper is organized as follows: the details of sample preparation and soft x-ray measurements are presented in Sec. II. The crystal structure of different compounds and their basic properties are summarized in Sec. III. Results of x-ray measurements for the whole series of BiMO_3 (M=Sc,Cr,Fe,Co,Ni) compounds and comparison with electronic-structure calculations are discussed in Sec. IV. The main conclusions are summarized in Sec. V.

II. EXPERIMENTAL DETAILS

All the samples were synthesized using a high-pressure, high-temperature method. Starting mixtures were placed in Au capsules and treated at 6 GPa in a belt-type high-pressure apparatus at different temperatures (heating rate was about 140 K/min). After heat treatment, the samples were quenched to room temperature, and the pressure was slowly released. $BiCrO_3$ was prepared from a 1:1 mixture of Bi_2O_3 (99.99%) and Cr_2O_3 (99.9%) at 1653 K for 60–70 min.[12] $BiMnO_3$ was prepared from a 1:1 mixture of Bi_2O_3 and Mn_2O_3 at 1383 K for 60–70 min.[13] Single-phased Mn_2O_3 was prepared by heating commercial MnO_2 (99.99%) in air at 923 K for 24 h. For the preparation of $BiScO_3$, stoichiometric mixtures of Bi_2O_3 and Sc_2O_3 (99.9%) were dried at 873 K for 8 h and then treated at 1413 K (at 6 GPa) for 40 min.[14]

For the preparation of $BiFeO_3$, stoichiometric mixtures of Bi_2O_3 and Fe_2O_3 (99.9%) were first annealed at ambient pressure at 1073 K for 2 h. This procedure gave a mixture of $BiFeO_3$ (about 70 wt %), $Bi_{25}FeO_{39}$, and $Bi_2Fe_4O_9$. The resulting mixture was treated at 1273 K (at 6 GPa) for 1 h. After the high-pressure treatment, single-phased $BiFeO_3$ was obtained. $BiCoO_3$ was synthesized from stoichiometric mixtures of Bi_2O_3, Co_3O_4 (99.9%), and $KClO_3$ at 1483 K (at 6 GPa) for 1 h, and $BiNiO_3$ from Bi_2O_3, NiO (99.9%), and $KClO_3$ at 1483 K (at 6 GPa) for 1 h. The resulting samples were reground, washed with water, dried, and repressed at about 1 GPa at room temperature.

The x-ray emission spectra (XES) were measured at beamline 8.0.1 at the Advanced Light Source (ALS) at the Lawrence Berkeley National Laboratory.[15] The x-ray absorption spectra (XAS) were measured at the Spherical Grating Monochromator beamline at the Canadian Light Source (CLS) at the University of Saskatchewan.[16] The O 1s XAS spectra were measured in the total fluorescence yield (TFY) mode, which provides more bulk sensitivity than electron yield methods do. All XAS measurements were normalized by the incident photon flux, measured by a highly-transparent gold mesh. The O $K\alpha$ XES was excited near the O 1s ionization threshold to suppress the high-energy satellite structure. The instrumental resolving power ($E/\Delta E$) was approximately 10^3 for the XES measurements and approximately 5×10^3 for the XAS measurements.

III. CRYSTAL STRUCTURE AND PHYSICAL PROPERTIES OF BiMO_3 COMPOUNDS

Within the multiferroic compounds, perovskite-type and related oxides are often the subject of extensive study. Below we give a short summary of crystal structure and basic physical properties of the BiMO_3 (M=Sc,Cr,Mn,Fe,Co,Ni) compounds. The space groups and lattice constants for the whole series are collected in Table I. The selected bond lengths are shown in Tables II–IV.

The structure of $BiScO_3$ has monoclinic symmetry with the space group $C2/c$.[14] $BiScO_3$ is nonmagnetic and most of the interest in this compound is in the ferroelectric properties

TABLE II. Selected bond lengths in $BiScO_3$, $BiCrO_3$, and $BiMnO_3$, in angstrom. $\Lambda=\frac{1}{N}\Sigma_1^N(\frac{l_i-l_{av}}{l_{av}})^2$ and $l_{av}=\frac{1}{N}\Sigma_1^N l_i$, where l_i is the ith bond.

	$BiScO_3$	$BiCrO_3$	$BiMnO_3$
M1-O2×2	2.08570	1.98308	1.90556
M1-O1×2	2.10990	1.99158	2.19906
M1-O3×2	2.15779	1.97805	1.98549
$\Lambda(M1\text{-O})$	2.0×10^{-4}	0.08×10^{-4}	37.2×10^{-4}
M2-O3×2	2.09607	1.97890	1.94151
M2-O1×2	2.11635	1.99268	1.92401
M2-O2×2	2.13574	2.01393	2.24174
$\Lambda(M2\text{-O})$	0.6×10^{-4}	0.5×10^{-4}	51.3×10^{-4}
Bi-O3	2.15352	2.25697	2.24562
Bi-O2	2.19212	2.23752	2.21778
Bi-O1	2.24633	2.32584	2.23928
Bi-O1	2.55437	2.44659	2.46625
Bi-O3	2.89682	2.65246	2.70996
Bi-O2	3.01816	2.78741	2.83703
Λ(Bi-O)	18.7×10^{-3}	37.0×10^{-3}	9.9×10^{-3}

TABLE III. Selected bond lengths in $BiFeO_3$ and $BiCoO_3$, in angstrom.

Fe-O×3	1.97139	Co-O1	1.71781
Fe-O×3	2.08310	Co-O2×4	2.01593
Λ(M-O)	8×10^{-4}		37×10^{-4}
Bi-O×3	2.30512	Bi-O2×4	2.25155
Bi-O×3	2.51513	Bi-O1×4	2.79852
Λ(Bi-O)	1.9×10^{-3}		11.7×10^{-3}

of the $BiScO_3$-$PbTiO_3$ system. For the well-known piezoelectric material $Pb(Zr,Ti)O_3$ (PZT), the Curie temperature T_C at the morthotropic phase boundary between the rhombohedral and tetragonal ferroelectric state is 386 °C. It has been shown that for $BiScO_3$-$PbTiO_3$, the T_C reaches 450 °C (Ref. 17) while the piezoelectric coefficients in bulk are comparable to those of commercial PZT.

$BiCrO_3$ crystallizes in an orthorhombic structure above 420 K with the space group *Pnma* and lattice parameters a =5.54568(12) Å, b=7.7577(2) Å, and c=5.42862(12) Å at 490 K.[12] A structural phase transition from an orthorhombic to a monoclinic structure occurs at 420 K.[12,18–20] Between 420 and 7 K, $BiCrO_3$ has a monoclinic structure with the space group $C2/c$ and a=9.4641(4) Å, b=5.4790(2) Å, c =9.5850(4) Å, β=108.568(3)° at 7 K.[12] A long-range G-type antiferromagnetic order with weak ferromagnetism develops below T_N=109 K and does not change down to 7 K.[12] Four anomalies of magnetic origin were observed at 40, 75, 109, and 111 K.[20] The magnetic moments of the Cr^{3+} ions were found to align along the monoclinic b axis in a similar manner to the direction of the magnetic moments of the Mn^{3+} in $BiMnO_3$.[21,22] The magnetic structure of $BiCrO_3$ was first predicted from *ab initio* electronic-structure calculations.[23]

The bismuth manganite ($BiMnO_3$) has a highly distorted perovskite structure and has been regarded as a multiferroic material. The ferroelectricity has been analyzed within first-principles electronic-structure calculations,[24] and attributed to the chemical activity of the Bi $6s^2$ lone pairs.[8] $BiMnO_3$ is the only ferromagnet among the discussed BiMO_3 compounds with a Curie temperature above 100 K. The largest saturation magnetization has been reported to be $3.92\mu_B$ per formula unit,[13] which is close to the $4\mu_B$ expected for the ferromagnetic state. The ferroelectric hysteresis loop has been observed in polycrystalline and thin-film samples of $BiMnO_3$,[25] although the measured ferroelectric polarization was much smaller (about 0.043 $\mu C/cm^2$ at 200 K) than the one obtained in the first-principles calculations for the experimental noncentrosymmetric structure (about 0.52 $\mu C/cm^2$).[26]

$BiMnO_3$ undergoes two phase transitions at temperatures 474 K (monoclinic to monoclinic) and 770 K (monoclinic to orthorhombic).[22,27,28] According to early experimental data, $BiMnO_3$ was considered to have noncentrosymmetric $C2$ space group below 770 K.[22,27] Recently, the crystal structure of $BiMnO_3$ was reexamined by Belik *et al.*[13] and confirmed by neutron powder-diffraction experiments by Montanari *et al.*[21] The new experiments reveal that $BiMnO_3$ below 770 K has a centrosymmetric $C2/c$ space group with parameters given in Table I. A structural optimization performed using modern methods of electronic-structure calculations has shown that the noncentrosymmetric $C2$ structure, which had been reported earlier converges to the new total-energy minimum corresponding to the $C2/c$ structure with zero net polarization.[29,30]

Since the $C2/c$ structure of $BiMnO_3$ has inversion symmetry, the hypothesis that electric polarization arises due to bismuth lone pairs is no longer valid. The magnetic mechanism of inversion symmetry breaking was considered recently in Ref. 31. It was shown that the peculiar orbital ordering realized below 474 K gives rise to ferromagnetic (FM) interactions between nearest-neighbor spins which compete with longer-range antiferromagnetic (AFM) interactions. The solution of the low-energy model for $3d$ states in $BiMnO_3$ revealed that the true symmetry is expected to be Cc. The solution of the realistic model indicates a noncollinear magnetic ground state, where the FM order along one crystallographic axis coexists with the hidden AFM order and a related ferroelectric polarization along two other axes.[32]

The perovskite $BiFeO_3$ is ferroelectric with T_c=1103 K and antiferromagnetic with T_N=643 K and a canted spin structure.[33] The bulk single crystal has a rhombohedrally distorted perovskite structure with the space group $R3c$ (Ref. 34) and lattice parameters presented in Table I. The G-type collinear antiferromagnetic spin configuration has been

TABLE IV. Selected bond lengths in $BiNiO_3$, in angstrom.

Ni1-O2×2	1.98294	Ni2-O3×2	2.04959	Ni3-O5×2	1.98075	Ni4-O1×2	2.05408
Ni1-O3×2	1.99200	Ni2-O4×2	2.07097	Ni3-O2×2	2.10662	Ni4-O6×2	2.10927
Ni1-O4×2	2.28697	Ni2-O1×2	2.13415	Ni3-O6×2	2.12071	Ni4-O5×2	2.20769
Λ(M-O)	46×10^{-4}		3×10^{-4}		9×10^{-4}		9×10^{-4}
Bi1-O3	2.21311	Bi2-O1	2.03349				
Bi1-O5	2.26541	Bi2-O4	2.04058				
Bi1-O2	2.32491	Bi2-O6	2.09686				
Bi1-O3	2.41745	Bi2-O2	2.13787				
Bi1-O1	2.52033	Bi2-O5	2.24213				
Bi1-O4	2.67658	Bi2-O6	2.25756				
Λ(Bi-O)	4.3×10^{-3}		1.7×10^{-3}				

modified by subjecting it to a long-range (620 Å) modulation leading to a spiral modulated spin structure.[35] The spontaneous polarization of a single crystal is 3.5 $\mu C/cm^2$ along (001) direction and 6.1 $\mu C/cm^2$ in (111) direction at 77 K.[36] This value is significantly smaller than spontaneous polarization of lead titanate (80–100 $\mu C/cm^2$ with the $T_C \sim 763$ K). However, the heteroepitaxially constrained thin films of $BiFeO_3$ display a room-temperature spontaneous polarization of 50–60 $\mu C/cm^2$, an order of magnitude higher than in the bulk.[37] The spin-polarized first-principles calculation within local spin-density approximation (LSDA) using the pseudopotential VASP package with the optimized lattice parameters for the bulk rhombohedral phase results in polarization of 6.61 $\mu C/cm^2$ in excellent agreement with experiment.[37] The thin films were shown to have tetragonal-like structure. For the *P*4*mm* symmetry and lattice parameters measured for thin film, the Berry-phase calculation[37] yields a spontaneous polarization of 63.2 $\mu C/cm^2$, consistent with experimental data, but it was revealed that small changes in lattice parameters can lead to a dramatically different polarization. The magnetoelectric coefficient (dE/dH, *E*–electric field, and *H*–magnetic field) was measured to be 3 V/cm Oe at zero field.[37] Later on, the values of remnant polarization were increased to 55 $\mu C/cm^2$ for (001) films, 80 $\mu C/cm^2$ for (101) films and about 100 $\mu C/cm^2$ for (111) films.[38] The $BiFeO_3$ films grown on (111) have the rhombohedral structure as single crystals whereas films grown on (101) or (001) are monoclinically distorted.[38] The highest remnant polarization ever measured for a ferroelectric material, 146 $\mu C/cm^2$, has been reported for $BiFeO_3$ thin films with tetragonal crystal structure in Ref. 39. A wide range of measured polarization values were shown to be consistent with the modern theory of polarization,[40–42] which recognizes that polarization is a lattice of values rather than a single vector.[43]

$BiCoO_3$ is isotypic with $BaTiO_3$ and $PbTiO_3$ and has a tetragonal crystal structure with the lattice parameters $a=3.71990(7)$ Å, $b=4.71965(15)$ Å, and $c/a=1.269$ at 5 K.[44] $BiCoO_3$ is an insulator with $T_N=470$ K. It has C-type antiferromagnetic order where the magnetic moments of the Co^{3+} ions aligning antiferromagnetically in the *ab* plane and antiferromagnetic *ab* layers stack ferromagnetically along the *c* axis.[44] The high-spin (HS) configuration of Co^{3+} ions ($S=2$) has been reported.[44] The magnetic moments are $m=3.24(2)\mu_B$ for $T=5$ K and $m=2.93(2)\mu_B$ at room temperature.[44] A reduction in the observed magnetic moment compared to the expected value $4\mu_B$ may be ascribed to the covalency of Co-O bonds. The bond valence sums (BVS) at 300K obtained in Ref. 44 were 3.14 for Bi and −2.13 for O2 corresponding to the oxidation states +3 and −2, respectively. The BVS values were 2.68 for Co and −1.57 for O1 indicating the covalency effects. The spontaneous polarization in $BiCoO_3$ of 179 $\mu C/cm^2$ has been predicted from first-principle Berry-phase calculations.[45] The experimental observation of a ferroelectric hysteresis loop is problematic since the resistivity appears too low for the large applied electric field. Therefore it was proposed that $BiCoO_3$ should be regarded as a pyroelectric rather than a ferroelectric material (in pyroelectrics the dipole moments cannot be reoriented by external electric field).[44] The C-type antiferromagnetic order with a reduced magnetic moment of $2.41\mu_B$ have been also predicted from first-principles calculations[45] resulting in insulating ground state with an energy gap of 0.6 eV.

$BiNiO_3$ has been found to be an insulating antiferromagnet ($T_N=300$ K) (Ref. 46) with a heavily distorted triclinic symmetry $P\bar{1}$. The lattice constants are shown in Table I. X-ray powder-diffraction data has revealed that Bi ions were disproportionately weighted toward Bi^{3+} and Bi^{5+} and therefore the oxidation state of the Ni ion was +2 rather than the expected +3.[46,47] The Curie constant estimated from the magnetic susceptibility of $BiNiO_3$ is close to that expected for $S=1$ rather than for $S=1/2$ system. This fact as well as BVS confirms the divalent nature of Ni. The electronic structure of $BiNiO_3$ has been performed by the full-potential method within local-density approximation (LDA) plus *U* ($U=8$ eV, $J=0.95$ eV) approximation with the G-type antiferromagnetic spin configuration.[48] At ambient pressure, an insulating solution with the charge-transfer gap of 0.8 eV was obtained in agreement with the value of 0.675 eV estimated from the electrical resistivity.[46] From the powder neutron-diffraction study, it was found that the valence state of $BiNiO_3$ changes under pressure.[48] Both neutron-diffraction measurements and BVS show that under pressure the charge disproportionate state melts leading to the simultaneous charge transfer from Ni to Bi so that the high-pressure phase is metallic $Bi^{3+}Ni^{3+}O_3$. This transition takes place at 4 GPa pressure and structure changes to the $GdFeO_3$ type with the *Pbnm* symmetry.[48] First-principles calculations also reproduce the metallic character of high-pressure phase.[48]

IV. RESULTS AND DISCUSSION

A. LSDA calculations

The electronic structure of the $BiMO_3$ ($M=Sc,Cr,Mn,Fe,Co,Ni$) series was calculated within the LSDA (Refs. 49 and 50) with a linear muffin-tin orbitals basis (LMTO) (Refs. 51 and 52) using the Stuttgart tight-binding-LMTO program (version LMTO47). The experimental atomic positions and lattice constants shown in Table I were used for all compounds, and the experimentally determined magnetic structures described in previous sections were used for the spin-polarized calculations (for $BiFeO_3$ the G-type AFM order was assumed). The calculated energy gaps (Δ_g^{calc}) and magnetic moments are shown in Table V along with the available experimental data. The LSDA approach indicates that $BiScO_3$, $BiCrO_3$, $BiFeO_3$, and $BiCoO_3$ are insulators. For $BiMnO_3$ and $BiNiO_3$, LSDA results in half-metallic and metallic solution, respectively, although both materials are known to be insulators. The failure of LSDA in these two cases is due to the improper treatment of Coulomb correlations. It is well known that LSDA+*U* improves the description of correlation effects in transition-metal oxides due to treating the strong Coulomb repulsion between localized *d* states by adding a Hubbard-type term to the effective potential.[53] This calculation requires the Hubbard parameter *U* and exchange interaction *J*. Although these parameters can be calculated by the constrained LDA

TABLE V. The calculated (Δ_g^{calc}) and estimated from XES and XAS spectra (Δ_g^{exp}) values of energy gap in comparison with the experimental data taken from literature ($\Delta_g^{Lit.}$). The error in the estimated energy gap Δ_g^{exp} is roughly ± 0.5 eV. The calculated magnetic moments on the M ion (m_M) along with experimental estimations ($m_M^{Lit.}$) for $BiMO_3$ compounds. The different values of magnetic moments in case of M =Cr,Mn,Ni correspond to the nonequivalent M atoms in the unit cell.

Compound	Δ_g^{calc} (eV)	Δ_g^{exp} (eV)	$\Delta_g^{Lit.}$ (eV)	m_M (μ_B)	$m_M^{Lit.}$ (μ_B)	Config. M^{3+}
BiScO3	3.3	2.6		0		d^0
$BiCrO_3$	0.88	1.4		2.63, 2.65	2.55[a]	d^3
$BiMnO_3$	0.33	0.9	Insulator[b]	3.65, 3.64	3.2[c]	d^4
$BiFeO_3$	0.51	0.9	1.3,[d] 2.5[e]	3.54	3.75[f]	d^5
$BiCoO_3$	0.72	1.7	Insulator[g]	2.41	3.24[g]	d^6
$BiNiO_3$	1.23	1.1	0.675[h]	1.7; 1.67	1.76[i]	d^7

[a]Reference 12.
[b]Reference 56.
[c]Reference 22.
[d]Reference 10.
[e]Reference 57.
[f]Reference 34.
[g]Reference 44.
[h]Reference 46.
[i]Reference 47.

method,[54] in the present work we just use the typical values $U=3$ eV, $J=1$ eV for $BiMnO_3$ (Ref. 31) and $U=8$ eV, $J=1$ eV for $BiNiO_3$.[55]

The partial densities of states (DOSs) calculated for the $BiMO_3$ series within the LSDA and LSDA+U (for $BiNiO_3$ and $BiMnO_3$) approaches are presented in Fig. 1. The valence band for all $BiMO_3$ compounds is formed by the M 3d states hybridized with the O 2p states. The low-energy states at about −10 eV come from Bi 6s states, the so-called lone pair. These states are only slightly hybridized with 2p states of oxygen.

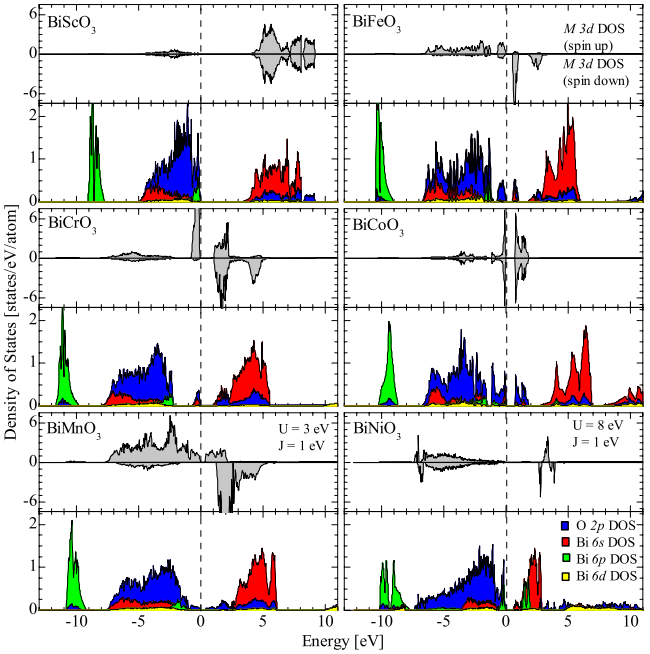

FIG. 1. (Color online) LSDA (LSDA+U with $U=3$ eV, $J=1$ eV for $BiMnO_3$, and $U=8$ eV, $J=1$ eV for $BiNiO_3$) partial M spin-resolved 3d, O 2p, and Bi 6s, 6p, and 6d density of states for $BiMO_3$ (M=Sc,Cr,Mn,Fe,Co,Ni) compounds. The Fermi level corresponds to zero.

$BiScO_3$, $BiCrO_3$, and $BiMnO_3$ all have a monoclinic structure and can be compared directly. The bond lengths for these three compounds are summarized in Table II. Although the space groups of these compounds are the same, the MO_6 octahedra distortions are different for each and most pronounced in the case of $BiMnO_3$. The parameter $\Lambda(M\text{-O})$ in Table II indicates the degree of MO_6 octahedra distortion. The largest $\Lambda(M\text{-O})$ corresponds to $BiMnO_3$ while in $BiCrO_3$, the CrO_6 octahedron is almost undistorted. The shortest Bi-O bond lengths also shrink from Sc to Mn. Since the oxygen atoms surrounding Bi do not form regular polyhedron, we take the six nearest neighbors and estimate the variations between the compounds [denoted by Λ(Bi-O)]. All three compounds display rather strong deviation from the average Bi-O bond but the largest Λ(Bi-O) is found for $BiScO_3$. $BiFeO_3$, and $BiCoO_3$ have different structures. Five oxygen atoms surrounding the Co ion form a pyramid (see Table III). This pyramid is contracted so the distortion parameter is rather large. In $BiFeO_3$, the FeO_6 octahedron is less distorted than in $BiMnO_3$ system. The oxygen atoms around Bi are distributed almost evenly in $BiFeO_3$ while in $BiCoO_3$ rather irregular arrangement of oxygen atoms can be seen from the Bi-O bond lengths shown in Table III. In Table IV, the distances between the Bi-O and the Ni-O bond lengths for $BiNiO_3$ are shown. The low symmetry of $BiNiO_3$ leads to the four nonequivalent Ni atoms and two nonequivalent Bi atoms in the unit cell. Among the four Ni octahedra formed by oxygen atoms, the one around Ni1 is the most distorted. The oxygen neighborhood around the Bi atoms is rather uniform.

For $BiScO_3$ and $BiCrO_3$, an insulating solution was obtained with LSDA calculations (see Fig. 1). $BiScO_3$ has a formal electronic configuration d^0 and calculated energy gap of 3.3 eV. The valence band is formed by O 2p states while the conduction band is composed of Sc 3d states hybridized with O 2p states. $BiCrO_3$ has three electrons occupying t_{2g} orbitals (see Fig. 1). The energy gap of 0.88 eV and magnetic moment of 2.63 and 2.65μ_B (for two nonequivalent Cr at-

oms) was obtained in spin-polarized calculation in good agreement with the value $2.55\mu_B$ obtained in neutron-diffraction experiments.[12] Both the valence and conduction bands are formed mainly by Cr $3d$ states with small admixture of O $2p$ states. LSDA+U predicts an insulating state for ferromagnetically ordered $BiMnO_3$ in agreement with experiment (see Fig. 1). The calculated magnetic moments for two nonequivalent Mn ions are $3.64\mu_B$ and $3.65\mu_B$, in agreement with experimental values shown in Table V. Both the O $2p$ and the Mn $3d$ bandwidths are wider than those of $BiCrO_3$ but the main contribution to the valence band comes from Mn $3d$ states. There is also a strong overlap of O $2p$ and Mn $3d$ bands.

LSDA calculations result in an insulating solution for $BiFeO_3$ with the energy gap of 0.51 eV. This is much smaller than experimental estimates.[10,57] However, the magnetic moment value of $3.54\mu_B$ is in good agreement with experiment (see Table V). The calculated DOS agrees well with the results of previous *ab initio* calculations.[43] Within LSDA, the HS state for the d^5 configuration of Fe ion was obtained as shown in Fig. 1. Both the valence and conduction bands are formed predominantly by Fe $3d$ states hybridized with O $2p$ states.

The LSDA calculations for $BiCoO_3$ suggest it is an insulator with an energy gap of 0.72 eV. We obtained HS state of d^6 electrons with magnetic moment of $2.41\mu_B$ which is smaller than $4\mu_B$ (expected for HS state) due to covalency effects.

With the LSDA+U method, $BiNiO_3$ is insulator with an energy gap of 1.23 eV. This value is twice as large as the experimental result from Ref. 46 but in good agreement with the present experimental estimation (see Table V). The values of the calculated magnetic moments given in Table V are in agreement with the experimental ones. From the density of states, it can be seen that the top of the valence band and the bottom of the conduction band are formed by Bi1 $6s$ and Bi2 $6s$ states hybridized with O $2p$ states. The occupancies calculated for the d states of the four nonequivalent Ni atoms in the LSDA+U calculation are 8.2, 8.36, 8.23, and 8.49 indicating that Ni has a 2+ valence which is in agreement with calculations performed in the literature.[48]

B. XES and XAS measurements

The O $K\alpha$ XES and O $1s$ XAS measurements of $BiMO_3$ (M=Sc,Cr,Mn,Fe,Co,Ni), which probe the occupied and vacant O $2p$ states, respectively, are presented in Fig. 2. The fine structure and energy distribution of the O $K\alpha$ XES matches the O $2p$ occupied DOS obtained from LSDA calculations (see Fig. 1). A small amount of hybridization between Bi $6s$ and O $2p$ states is visible at about 519 eV in all compounds, as suggested by the calculated O $2p$ states.

As we have shown in Ref. 58, there is significant hybridization between the O $2p$ states and the occupied d states of nontransition-metal cations. This hybridization is involved in formation of chemical bonding in solids. In $BiMO_3$ compounds, as seen in Fig. 1, the main maxima of O $2p$ and Bi $6d$ states occur at the same energy. The main maxima of the calculated M $3d$ states are also close to that energy. The

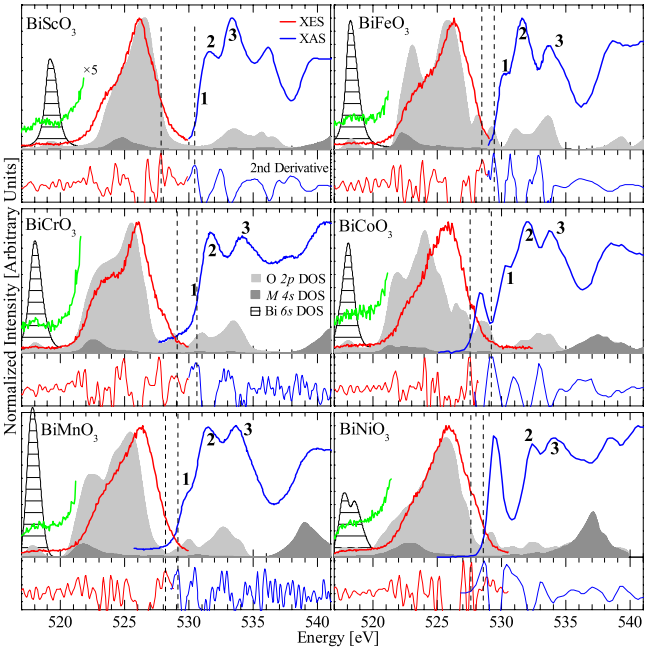

FIG. 2. (Color online) Measured oxygen $K\alpha$ XES and O $1s$ XAS of $BiMO_3$ compounds. The XAS is measured in total fluorescent yield (TFY) mode. The energy gap is estimated using the peaks in the second derivative, plotted below the corresponding spectra. The Bi $6s$-O $2p$ hybridization peak at about 519 eV has been magnified by a factor of 5. The M $4s$, O $2p$, and Bi $6s$ DOS are shaded in the background of each figure (for M=Sc,Cr,Mn,Fe,Co,Ni). They have been convoluted with a 0.3 eV wide Lorentzian function to mimic the experimental resolution. The Fermi level for the DOS was estimated using the peak in the XES second derivative.

nonbonding localized $3d$ states weakly mix with O $2p$ states near the Fermi level.

All O $K\alpha$ XES spectra consist of a low-energy subband located at ~2.5 eV with respect to the main maximum. As shown in Ref. 58, the low-energy subband of O $K\alpha$ XES of all binary oxides is directly connected with the s valence states of the cation. The energy separation of this subband from the main valence band depends on the period number of the transition metal. For ZnO, it is ~2.4 eV, which coincides with the separation of the subband from the main band of O $K\alpha$ XES for $BiMO_3$ compounds. The Bi $6s$ states are located ~5 eV below the M $4s$ states, and therefore hybridize only weakly with the O $2p$ states (see Fig. 1).

The near-edge fine structure of the O $1s$ XAS (see Fig. 2) consists of three peaks (labeled as 1, 2, and 3) separated by ~1.5–2 eV for all compounds. There is a similar peak structure in the calculated unoccupied O $2p$ DOS (Fig. 2) in spite of the fact that the experimental energy gap (Δ_g^{exp}) is not reproduced in LSDA calculations. Indeed, the lack of the appropriate energy gap does not affect the correct reproduction of the energy distance between the main maximum of the O $K\alpha$ XES and the first peak of the O $1s$ XAS (~5 eV) in the LSDA calculations. This further demonstrates the well-known fact that O $2p$ states are less influenced by correlation effects than d states.[59]

The O $1s$ XAS spectra of $BiNiO_3$ and $BiCoO_3$ show additional peaks near the Fermi level similar to those which

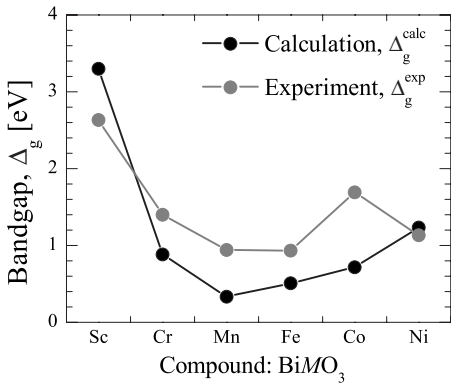

FIG. 3. The experimental (gray dots) and calculated (black dots) energy gaps for the BeMO_3 compounds.

were observed in the O 1*s* XAS of $Li_xNi_{1-x}O$,[60] $LiCoO_2$,[61] and $LaNiO_3$.[62] These additional peaks were attributed in Refs. 60 and 62 to the formation of O 2*p* hole electronic states because of the energy disadvantage associated with a Ni^{3+} charge state. The Co^{3+} charge state is more stable, hence the intensity of the holelike peak in $BiCoO_3$ is much lower than that in $BiNiO_3$. Indeed, the "hole effect" in $BiNiO_3$ is even larger than that in $Li_xNi_{1-x}O$.[60] Among the materials studied in Ref. 60, the intensity of the O 2*p* hole peak was found to be largest for $Li_{0.5}Ni_{0.5}O$ where the hole peak had ~70% of the intensity of the main maximum of the O 1*s* XAS. Similar intensity ratios have been reported for $LaNiO_3$.[62] In $BiNiO_3$, however, the relative intensity of the O 2*p* hole peak is about 100% of the intensity of the main O 2*p* band. The O 2*p* holes are created in order to maintain the neutrality of the compound with the Ni^{2+} valence state. They are clearly observed in the O 1*s* XAS for Ni oxides $LaNiO_3$ and $BiNiO_3$. In the LSDA+*U* calculation, the gap arises between the states predominantly formed by Bi 6*s* states strongly hybridized with O 2*p* states. The Ni atoms have a 2+ valency in agreement with our experimental findings.

The energy gap for all compounds in the series was estimated using the peaks in the second derivative. This method has been shown to work well with O *Kα* XES and 1*s* XAS.[59] The estimated energy gaps from the experimental spectra and the calculations are not exactly the same. This is expected since LSDA calculations are known to underestimate the energy gap by up to 50%, and the "second derivative method" can often overestimate the energy gap when there are only a few states near the Fermi level (as is the case with $BiMnO_3$). We have found that the calculated energy gaps are mostly within 0.5 eV of the experimental energy gaps and, more importantly, the trend in the calculated energy gaps is essentially the same as that in the experimental energy gaps for these materials (see Fig. 3).

Note that the choice for the peak in the second derivative for the O 1*s* XAS in $BiCoO_3$ and $BiNiO_3$ is somewhat arbitrary since the O 2*p* hole peak obscures the true absorption onset. In these two cases, the second derivative method is not really applicable to the O 1*s* XAS; even though the estimated energy gap for $BiNiO_3$ is the same as the calculated value. Second, it is worthwhile to point out that $BiCoO_3$ and

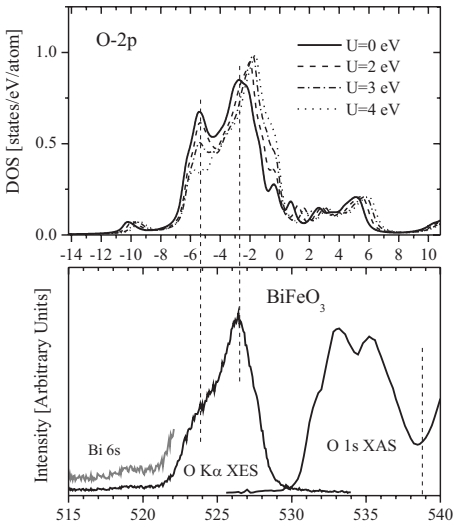

FIG. 4. The comparison between the O *Kα* XES and O 1*s* XAS (lower panel) and the LSDA+*U* O 2*p* DOS (upper panel) of $BiFeO_3$. In the upper panel, the calculated LSDA+*U* O 2*p* DOSs for several values of *U* are shown. The O 2*p* DOSs have been convoluted with the Fermi step at $T=300$ K and broadened by 0.3 eV using a Lorentzian to mimic the experimental resolution. The Fermi level corresponds to zero.

$BiMnO_3$, which exhibit the largest and second largest discrepancy between calculated and experimentally estimated energy gaps, also exhibit the largest and second largest discrepancy between the estimated (using the peak of the second derivative in the XES spectra) and the calculated Fermi level, as shown in Fig. 2 (note that even though the 2*p* hole peak obscures the absorption onset, we still expect the second derivative to predict the Fermi level from the O *Kα* XES spectra). Since the shape, if not the estimated energy placement, of the calculated O 2*p* DOS is still a good match to the measured O *Kα* XES, the discrepancy in the energy gaps is likely a combination of the inability of the LSDA calculations to accurately predict gaps and the ambiguity in the onset of the measured XES.

The comparison of the oxygen and iron x-ray spectra of $BiFeO_3$ with the calculated O 2*p* and Fe 3*d* DOSs is shown in Figs. 4 and 5, respectively. The Fermi-level position for the Fe L_3 XES was determined using the x-ray photoemission spectroscopy (XPS) Fe $2p_{3/2}$ binding energy (710 eV).[63] In the absence of XPS O 1*s* data, the O K_α XES is compared with O 2*p* DOS by alignment of Bi 6*s* related subbands. The LSDA calculation reproduces the energy position of the Fe L_3 XES (which probes occupied Fe 3*d* states) with respect to the Fermi level. On the other hand, the available LSDA+*U* calculations[10,43] show a low-energy shift of Fe 3*d* band which contradicts the experimental Fe L_3 XES. The spectral weight of Fe 3*d* and O 2*p* states is redistributed with increasing *U* value within LSDA+*U* calculations, as shown in Figs. 4 and 5. As the *U* value rises, the Fe 3*d* states are shifted to lower energies (Fig. 5). At the same time, the O 2*p* states (Fig. 4) are shifted toward Fermi level. Taking this trend into account, both the occupied O 2*p* and Fe 3*d* states obtained with $U=0$ eV are in better agreement with experimental spectra than the one calculated with a nonzero *U*. The

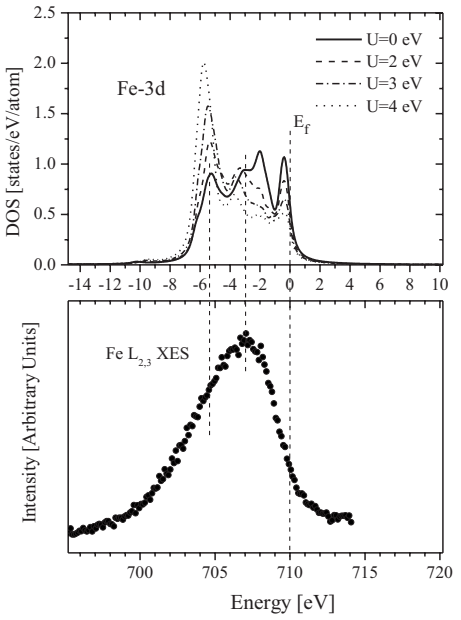

FIG. 5. The comparison between the Fe $L_{2,3}$ XES (lower panel) and the LSDA+U Fe 3d DOS (upper panel) of $BiFeO_3$. In the upper panel, the calculated LSDA+U Fe 3d DOSs for several values of U are shown. The Fe 3d DOSs have been convoluted with the Fermi step at $T=300$ K and broadened by 0.3 eV using a Lorentzian to mimic the experimental resolution. The Fermi level corresponds to zero.

Fe $L_{2,3}$ XES spectrum has some intensity at and just below the Fermi level while the O $K\alpha$ XES spectrum indicates a clear energy gap (see the lower panel of Fig. 4) in this energy region. In a recently published paper,[10] it was concluded that LSDA+U calculations ($U=2$ eV) are a better match to experimental Fe L_3 XES of $BiFeO_3$ than an LSDA (where $U=0$ eV) calculation. However, the comparison procedures used in matching calculations to experimental spectra are not described in Ref. 10. Based on the comparison from Ref. 10, one can estimate an XPS Fe $2p_{3/2}$ binding energy of 713 eV which contradicts the available experimental data (710 eV).[63]

We now turn to discussing the origin of ferroelectricity in $BiMnO_3$ and $BiFeO_3$. From Fig. 2 it is clear that the Bi 6s states in all compounds are not hybridized with the Bi 6p states. As was mentioned in Refs. 7 and 8, these Bi 6s lone pairs are slightly hybridized with O 2p states, and can induce a dipole moment. However, we could not find any difference in the degree of Bi 6s-O 2p hybridization for $BiMnO_3$ and $BiFeO_3$ compared to that of other BiMO_3 compounds where no ferroelectricity is observed.

A detailed comparison of the lone-pair localization and bonding for Sn^{2+}, Pb^{2+} and Bi^{3+} in $SnWO_4$, $PbWO_4$, and $BiVO_4$ has been carried out in Ref. 7. It was found that hybridization produces largely nonbonding lobe of localized electron density of Sn 5s-O 2p-Sn 5p orbital that is strongly stereochemically active. By calculating the cooperative orbital Hamiltonian overlap, it was shown that the lone-pair distortion leads to a significant increase in the Sn 5s-O 2p bonding interaction. Due to the relativistic contraction going from Sn^{2+} to Pb^{2+}, the Pb 5s-O 2p interaction is reduced. As a result, the symmetric structure is stabilized. Though for Bi^{3+} there is further stabilization of 6s orbitals, the stereoactive lone-pair distortion appears to be enhanced.[7] In the present paper, we analyze the similar tendency in BiMO_3 series trying to bind the Bi 6s-O 2p hybridization with the ferroelectricity. We obtained almost the same hybridization strength for all compounds indicating that lone pairs are active. Only in $BiNiO_3$, the Bi 6s-O 2p bonding states are less localized than those in the other compounds. The stereochemical activity of the Bi lone pair induces the electric moment but if the symmetry of the system includes inversion the net polarization turns to zero.

The first-principles calculations predicted the electric polarization of $P=47$ $\mu C/cm^2$ for the rhombohedral phase of $BiScO_3$ (Ref. 64) but afterward the crystal structure was experimentally detected as a centrosymmetric monoclinic $C2/c$.[14] Antiferroelectricity in $BiCrO_3$ was experimentally observed for the epitaxial films[65] ($P\sim 12$ $\mu C/cm^2$). Previously the A-type antiferromagnetic ground state and the distorted antiferroelectric structure have been proposed for $BiCrO_3$ based on the first-principles calculation.[23] This hardly makes $BiCrO_3$ a technologically relevant multiferroic material. $BiMnO_3$ is experimentally established ferroelectric system. The ferroelectric hysteresis loop has been observed on both polycrystalline and thin-film samples ($P\sim 0.043$ $\mu C/cm^2$).[25] The first-principles calculations resulted in polarization $P=0.52$ $\mu C/cm^2$ for the crystal structure $C2$, which does not include inversion symmetry[26] but recently the centrosymmetric $C2/c$ space group was detected.[13,21] $BiFeO_3$, the most well-studied multiferroic, has a spontaneous polarization of $P=6.1$ $\mu C/cm^2$ for single crystal[36] and much more impressive value of $P=50-60$ $\mu C/cm^2$ for thin films.[37] The theoretical calculations achieve $P=6.61$ $\mu C/cm^2$ in excellent agreement with experiment.[37] For $BiCoO_3$, *ab initio* calculations[45] predicted the $P=179$ $\mu C/cm^2$ though there is a lack of experimental confirmation so far. There is no experimental evidence for $BiNiO_3$ being multiferroic.[66] The highly distorted triclinic structure of $BiNiO_3$ (Ref. 46) is centrosymmetric, and therefore not polar. Strain in thin films or doping in bulk might contribute to the inversion symmetry breaking but this is the scope for the feature investigations.

It can be seen that among BiMO_3 (M=Sc,Cr,Mn,Fe,Co,Ni) series, there are two possible candidates for multiferroics: $BiFeO_3$ and $BiCoO_3$ since their space groups are noncentrosymmetric and hence allow the net polarization. Experimental results have thus far revealed two ferroelectrics in the series, namely, $BiFeO_3$ and $BiMnO_3$. The space group for the monoclinic structure of $BiMnO_3$ contains inversion while the rhombohedral $BiFeO_3$ has $R3c$ symmetry without inversion. Therefore, the origin of ferroelectricity in these two compounds seems to be different. As was recently proposed, the emergence of electric moment in $BiMnO_3$ is connected with inversion symmetry breaking by the noncollinear AFM order induced by particular orbital order below $T=474$ K.[31,32] Another scenario for the onset of ferroelectricity is possible in $BiFeO_3$: an extensive investigation of ferroelectricity in $BiFeO_3$ within the framework of density-functional theory was reported in Ref. 43. It was mentioned that the driving force of the ferroelectric distortion is the Bi lone pair. The calculated values of polarization

agree well with experimental results.[37] For $BiCoO_3$ with tetragonal structure the ferroelectric hysteresis loop has not yet been observed. One possible reason could be a low resistivity to the applied electric field as was pointed out in Ref. 44.

V. SUMMARY

In conclusion, the electronic structure of the BiMO_3 (M =Sc,Cr,Mn,Fe,Co,Ni) series was studied by soft x-ray emission and absorption spectroscopy. Experimental spectra were found to be in good agreement with spin-polarized electronic-structure calculations. The presence of holes in the O 1s XAS spectrum of $BiNiO_3$ was attributed to the 2+ valency of Ni. For all BiMO_3 (M=Sc,Cr,Mn,Fe,Co,Ni) compounds, the band-gap values were estimated from O $K\alpha$ XES and O 1s XAS spectra. In the case of $BiFeO_3$, this estimation results in the band-gap value ~0.9 eV. The x-ray spectra for multiferroic and nonmultiferroic compounds in the series do not reveal any difference in degree of Bi 6s-O 2p hybridization. It was concluded that for nonzero electric polarization, the stereochemical activity of the Bi lone pair should be accompanied with the inversion symmetry breaking. This condition is satisfied in the case of $BiMnO_3$, $BiFeO_3$, and $BiCoO_3$ but the electric polarization arises due to the different reasons. In $BiMnO_3$, noncollinear magnetic order with an AFM component breaks the inversion symmetry and allows net polarization. In $BiFeO_3$, the rhombohedral crystal structure does not contain inversion and the crucial role is played by Bi lone pairs. $BiCoO_3$ is supposed to be ferroelectric but a ferroelectric hysteresis loop has not yet been observed, therefore $BiCoO_3$ should be considered a pyroelectric material.

ACKNOWLEDGMENTS

We acknowledge the support of the Russian Science Foundation for Basic Research (Projects No. 08-02-00148 and No. 10-02-96011), the Dynasty Foundation (PZV), the Natural Sciences and Engineering Research Council of Canada (NSERC), and the Canada Research Chair program.

*john.mcleod@usask.ca
†pzv@ifmlrs.uran.ru

[1] G. Smolenskiĭ, V. Isupov, A. Agranovskaya, and N. Kranik, Sov. Phys. Solid State **2**, 2651 (1961).
[2] G. Smolenskiĭ, V. Yudin, E. Sher, and Y. E. Stolypin, Sov. Phys. JETP **16**, 622 (1963).
[3] J. F. Scott, Nature Mater. **6**, 256 (2007).
[4] N. A. Spaldin and M. Fiebig, Science **309**, 391 (2005).
[5] D. Khomskii, J. Magn. Magn. Mater. **306**, 1 (2006).
[6] D. Khomskii, Phys. **2**, 20 (2009).
[7] M. W. Stoltzfus, P. M. Woodward, R. Seshadri, J.-H. Klepeis, and B. Bursten, Inorg. Chem. **46**, 3839 (2007).
[8] R. Seshadri and N. A. Hill, Chem. Mater. **13**, 2892 (2001).
[9] C. Ederer and N. A. Spaldin, Curr. Opin. Solid State Mater. Sci. **9**, 128 (2005).
[10] T. Higuchi *et al.*, Phys. Rev. B **78**, 085106 (2008).
[11] J.-S. Kang, S. W. Han, J.-G. Park, S. C. Wi, S. S. Lee, G. Kim, H. J. Song, H. J. Shin, W. Jo, and B. I. Min, Phys. Rev. B **71**, 092405 (2005).
[12] A. A. Belik, S. Iikubo, K. Kodama, N. Igawa, S. Shamoto, and E. Takayama-Muromachi, Chem. Mater. **20**, 3765 (2008).
[13] A. A. Belik *et al.*, J. Am. Chem. Soc. **129**, 971 (2007).
[14] A. A. Belik *et al.*, J. Am. Chem. Soc. **128**, 706 (2006).
[15] J. J. Jia *et al.*, Rev. Sci. Instrum. **66**, 1394 (1995).
[16] T. Regier, J. Krochak, T. K. Sham, Y. F. Hu, J. Thompson, and R. I. R. Blyth, Nucl. Instrum. Methods Phys. Res. A **582**, 93 (2007).
[17] R. E. Eitel, C. A. Randall, T. R. Shrout, P. W. Rehrig, W. Hackenberger, and S.-E. Park, Jpn. J. Appl. Phys. **40**, 5999 (2001).
[18] F. Sugawara, S. Iiida, Y. Syono, and S. Akimoto, J. Phys. Soc. Jpn. **25**, 1553 (1968).
[19] S. Niitaka, M. Azuma, M. Takano, E. Nishibori, M. Takata, and M. Sakata, Solid State Ionics **172**, 557 (2004).
[20] A. A. Belik, N. Tsujii, H. Suzuki, and E. Takayama-Muromachi, Inorg. Chem. **46**, 8746 (2007).
[21] E. Montanari, G. Calestani, L. Righi, E. Gilioli, F. Bolzoni, K. S. Knight, and P. G. Radaelli, Phys. Rev. B **75**, 220101(R) (2007).
[22] A. Moreira dos Santos, A. K. Cheetham, T. Atou, Y. Syono, Y. Yamaguchi, K. Ohoyama, H. Chiba, and C. N. R. Rao, Phys. Rev. B **66**, 064425 (2002).
[23] N. A. Hill, P. Battig, and C. Daul, J. Phys. Chem. B **106**, 3383 (2002).
[24] N. A. Hill and K. M. Rabe, Phys. Rev. B **59**, 8759 (1999).
[25] A. Moreira dos Santos, S. Parashar, A. R. Raju, Y. S. Zhao, A. K. Cheetham, and C. N. R. Rao, Solid State Commun. **122**, 49 (2002).
[26] T. Shishidou, N. Mikamo, Y. Uratani, F. Ishii, and T. Oguchi, J. Phys.: Condens. Matter **16**, S5677 (2004).
[27] T. Atou, H. Chiba, K. Ohoyama, Y. Yamaguchi, and Y. Syono, J. Solid State Chem. **145**, 639 (1999).
[28] E. Montanari, G. Calestani, A. Migliori, M. Dapiaggi, F. Bolzoni, R. Cabassi, and E. Gilioli, Chem. Mater. **17**, 6457 (2005).
[29] T. Shishidou (private communication).
[30] P. Baettig, R. Seshadri, and N. A. Spaldin, J. Am. Chem. Soc. **129**, 9854 (2007).
[31] I. V. Solovyev and Z. V. Pchelkina, New J. Phys. **10**, 073021 (2008).
[32] I. V. Solovyev and Z. V. Pchelkina, Pis'ma Zh. Eksp. Teor. Fiz. **89**, 701 (2009) [JETP Lett. **89**, 597 (2009)].
[33] G. A. Smolenskiĭ and I. E. Chupis, Sov. Phys. Usp. **25**, 475 (1982).
[34] I. Sosnowska, W. Schäfer, W. Kockelmann, K. H. Andersen, and I. O. Troyanchuk, Appl. Phys. A **74**, s1040 (2002).
[35] I. Sosnowska, T. Peterlin-Neumaier, and E. Steichele, J. Phys. C **15**, 4835 (1982).
[36] J. R. Teague, R. Gerson, and W. J. James, Solid State Commun. **8**, 1073 (1970).
[37] J. Wang *et al.*, Science **299**, 1719 (2003).
[38] J. Li, J. Wang, M. Wuttig, and R. Ramesh, Appl. Phys. Lett. **84**, 5261 (2004).

[39] K. Y. Yun, D. Ricinschi, T. Kanashima, M. Noda, and M. Okuyama, Jpn. J. Appl. Phys. **43**, L647 (2004).
[40] R. D. King-Smith and D. Vanderbilt, Phys. Rev. B **47**, 1651 (1993).
[41] D. Vanderbilt and R. D. King-Smith, Phys. Rev. B **48**, 4442 (1993).
[42] R. Resta, Rev. Mod. Phys. **66**, 899 (1994).
[43] J. B. Neaton, C. Ederer, U. V. Waghmare, N. A. Spaldin, and K. M. Rabe, Phys. Rev. B **71**, 014113 (2005).
[44] A. A. Belik, S. Iikubo, K. Kodama, N. Igawa, S. Shamoto, S. Niitaka, M. Azuma, M. Takano, F. Izumi, and E. Takayama-Muromachi, Chem. Mater. **18**, 798 (2006).
[45] Y. Uratani, T. Shishidou, F. Ishii, and T. Oguchi, Jpn. J. Appl. Phys. **44**, 7130 (2005).
[46] S. Ishiwata, M. Azuma, M. Takano, E. Nishibori, M. Takata, M. Sakata, and K. Kato, J. Mater. Chem. **12**, 3733 (2002).
[47] S. J. E. Carlsson, M. Azuma, Y. Shimakawa, M. Takano, A. Hewat, and J. P. Attfield, J. Solid State Chem. **181**, 611 (2008).
[48] M. Azuma, S. Carlsson, J. Rodgers, M. G. Tucker, M. Tsujimoto, S. Ishiwata, S. Isoda, Y. Shimakawa, M. Takano, and J. P. Attfield, J. Am. Chem. Soc. **129**, 14433 (2007).
[49] W. Kohn and L. J. Sham, Phys. Rev. **140**, A1133 (1965).
[50] L. Hedin and B. I. Lundqvist, J. Phys. C **4**, 2064 (1971).
[51] O. K. Andersen, Phys. Rev. B **12**, 3060 (1975).
[52] O. Gunnarsson, O. Jepsen, and O. K. Andersen, Phys. Rev. B **27**, 7144 (1983).
[53] V. I. Anisimov, F. Aryasetiawan, and A. I. Lichtenstein, J. Phys.: Condens. Matter **9**, 767 (1997).
[54] O. Gunnarsson, O. K. Andersen, O. Jepsen, and J. Zaanen, Phys. Rev. B **39**, 1708 (1989).
[55] V. I. Anisimov, J. Zaanen, and O. K. Andersen, Phys. Rev. B **44**, 943 (1991).
[56] T. Kimura, S. Kawamoto, I. Yamada, M. Azuma, M. Takano, and Y. Tokura, Phys. Rev. B **67**, 180401(R) (2003).
[57] F. Gao, Y. Yuan, K. F. Wang, X. Y. Chen, F. Chen, J.-M. Liu, and Z. F. Ren, Appl. Phys. Lett. **89**, 102506 (2006).
[58] J. McLeod, R. Wilks, N. Skorikov, L. Finkelstein, M. Abu-Samak, E. Kurmaev, and A. Moewes, arXiv:0908.1581 (unpublished).
[59] E. Z. Kurmaev, R. G. Wilks, A. Moewes, L. D. Finkelstein, S. N. Shamin, and J. Kuneš, Phys. Rev. B **77**, 165127 (2008).
[60] P. Kuiper, G. Kruizinga, J. Ghijsen, G. A. Sawatzky, and H. Verweij, Phys. Rev. Lett. **62**, 221 (1989).
[61] V. R. Galakhov, V. V. Karelina, D. G. Kellerman, V. S. Gorshkov, N. A. Ovechkina, and M. Neumann, Phys. Solid State **44**, 266 (2002).
[62] M. Abbate, G. Zampieri, F. Prado, A. Caneiro, J. M. Gonzalez-Calbet, and M. Vallet-Regi, Phys. Rev. B **65**, 155101 (2002).
[63] P. Kharel, S. Talebi, B. Ramachandran, A. Dixit, V. M. Naik, M. B. Sahana, R. Naik, M. S. R. Rao, and G. Lawes, J. Phys.: Condens. Matter **21**, 036001 (2009).
[64] J. Íñiguez, D. Vanderbilt, and L. Bellaiche, Phys. Rev. B **67**, 224107 (2003).
[65] D. H. Kim, H. N. Lee, M. Varela, and H. M. Christen, Appl. Phys. Lett. **89**, 162904 (2006).
[66] G. Catalan, Phase Transitions **81**, 729 (2008).